Desalination 623 (2026) 119853

Contents lists available at ScienceDirect

Desalination

journal homepage: www.elsevier.com/locate/desal

Heteroepitaxial growth of DDR zeolite membranes for pervaporation dehydration of hypersaline LiBr solutions

Zilin Pan, Feng Ye *, Shuanshi Fan, Yanhong Wang, Xuemei Lang, Lisha Lu, Gang Li *

School of Chemistry and Chemical Engineering, South China University of Technology, Guangzhou, 510641, China

HIGHLIGHTS

- A heteroepitaxial growth method is developed to fabricate DDR zeolite membranes.
- Using a CHA zeolite seed layer significantly improves the membrane quality.
- DDR zeolite membranes are effective in dehydrating hypersaline LiBr solutions.
- A novel membrane-based desorbers in absorption chilling systems is proposed.

GRAPHICAL ABSTRACT

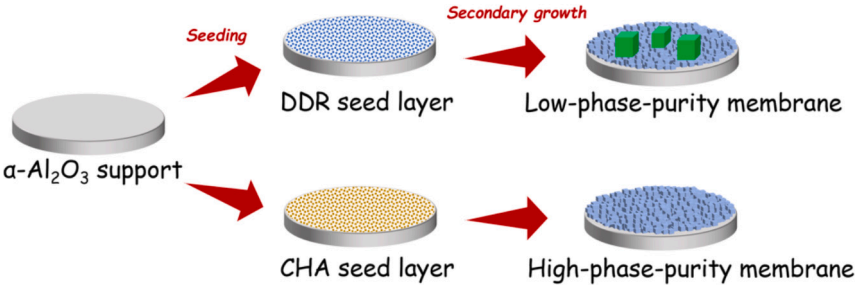

ARTICLE INFO

Keywords:
Zeolite membrane
DDR
Pervaporation dehydration
Lithium bromide
Membrane separation
Absorption chiller
Heteroepitaxial growth

ABSTRACT

LiBr-H_2O absorption chillers offer significant advantages in cooling applications; however, their widespread implementation has been severely limited by their large weight and size. The miniaturization of their key components is therefore critical to expanding their practical applications. This study presents a novel desorber design that employs a pervaporation process to concentrate LiBr solutions using DDR zeolite membranes. High-quality DDR zeolite membranes were fabricated via a heteroepitaxial growth process, utilizing CHA rather than DDR zeolite seeds, owing to the successful suppression of the SGT competitive phase during membrane synthesis. The resulting DDR zeolite membrane exhibited a water flux ranging from 0.16 to 1.56 $kg{\cdot}m^{-2}{\cdot}h^{-1}$ and a LiBr rejection exceeding 99.9 % for 20–60 wt% LiBr solutions at temperatures of 20–80 °C. The activation energy for water permeation decreased from 20.64 to 9.69 $kJ{\cdot}mol^{-1}$ as the LiBr concentration increased from 20 to 60 wt%, which stemmed primarily from the combined effect of the thermodynamic properties of LiBr solutions and the adsorption behaviors of the membrane. Moreover, the DDR zeolite membrane demonstrated excellent stability in the pervaporation dehydration of LiBr solutions, even at 80 °C, highlighting its potential for use in desorbers for LiBr-H_2O absorption chillers.

1. Introduction

Growing concerns regarding global warming and ozone layer depletion have spurred significant interest in LiBr-H_2O absorption chillers [1–3]. These systems utilize water as an environmentally benign refrigerant, offering a sustainable alternative to conventional compression chillers that rely on refrigerants with high global warming potential (GWP) and ozone-depleting properties, such as chlorofluorocarbons

* Corresponding authors.
E-mail addresses: fye9105@scut.edu.cn (F. Ye), fegli@scut.edu.cn (G. Li).

https://doi.org/10.1016/j.desal.2026.119853
Received 18 November 2025; Received in revised form 27 December 2025; Accepted 3 January 2026
Available online 4 January 2026

(CFCs) [4], hydrochlorofluorocarbons (HCFCs) [5,6], and hydrofluorocarbons (HFCs) [7,8]. Nevertheless, the widespread adoption of current LiBr–H_2O absorption chillers remains limited by their substantial weight and large footprint [9,10]. These challenges stem largely from the extensive use of conventional heat exchangers in key components including desorbers (also known as generators), absorbers, and economizers.

Among these components, the desorber, a key unit responsible for separating water from the LiBr–H_2O solution, has been a major focus of research aimed at system miniaturization [11–13]. In this context, membrane-based separation technologies have emerged as a promising alternative to traditional boiling desorption [14–16]. Membrane distillation, for instance, has been widely explored for this purpose using polymeric membranes [17–20]. Given the high salinity of LiBr–H_2O solutions, pervaporation is particularly well-suited for dehydration, showing significant potential for enabling novel, compact desorber designs. However, no studies have yet applied pervaporation to the dehydration of hypersaline LiBr solutions.

Zeolite membranes, recognized for their well-defined pore structures along with excellent thermal and chemical stability, are considered promising materials for separation applications [21]. Several types, including LTA [22,23], MFI [24], FAU [25], and CHA [26], have been developed for pervaporation desalination. Notably, Yu et al. [27] reported high water fluxes of 24 and 28 $kg{\cdot}m^{-2}{\cdot}h^{-1}$ using ultrathin CHA and FAU zeolite membranes, with thicknesses of only 600 nm and 500 nm, respectively, during the desalination of a 30 $g{\cdot}L^{-1}$ NaCl solution, demonstrating their strong potential in water/salt separation. However, current research has primarily focused on systems with relatively low salt concentrations (<5 wt%), which differ significantly from the highly concentrated LiBr solutions (50–60 wt%) used in LiBr-H_2O absorption chillers [28]. Owing to its narrow pore dimensions (0.36 nm × 0.44 nm) [29], which are comparable to those of CHA zeolite (0.38 nm × 0.38 nm) [30], the DDR zeolite membrane represents a potential candidate for pervaporation dehydration of highly concentrated LiBr solutions. Nevertheless, to the best of our knowledge, no prior study has applied a zeolite membrane-based pervaporation process for the dehydration of hypersaline LiBr solutions. Moreover, the synthesis of high-quality DDR zeolite membranes is often hindered by the formation of phase impurities such as DOH and SGT during membrane growth [31–37], which can substantially degrade separation performance.

This study developed a heteroepitaxial growth technique using CHA zeolite seeds to synthesize DDR zeolite membranes with high phase purity. Comparative analysis revealed the critical role of the seed layer, showing that CHA seeds effectively suppress the formation of competing SGT phases compared to conventional DDR seeds. The resulting high-quality membranes exhibited excellent performance in pervaporation dehydration of LiBr solutions, thereby demonstrating strong potential for novel membrane-based desorbers in LiBr–H_2O absorption chillers.

2. Experimental

2.1. Materials

Porous α-Al_2O_3 discs (porosity: 40%; diameter: 25 mm; average pore size: 100 nm) were used as supports for membrane fabrication. Silica sols (40 wt% in water) were purchased from Sigma-Aldrich. Sodium hydroxide (97 wt%) and 1-adamantanamine (ADA) (97 wt%) were purchased from Aladdin. USY zeolite (Si/Al = 40) and *N*, *N*, *N*-trimethyl-1-adamantylammonium hydroxide (TMAdaOH) (25 wt% in water) were purchased from Macklin. Ethylenediamine (EDA) (99 wt%) was provided by Guangdong Guangshi Reagent Technology Co., Ltd. All chemicals were used as received without further purification.

2.2. Synthesis of DDR and CHA zeolite seeds

Submicron DDR zeolite seeds were synthesized through a combination of hydrothermal crystallization and mechanical milling processes. Initially, a solution was prepared by dissolving NaOH and ADA in deionized water under continuous stirring until complete dissolution. Silica sols (40 wt%) were then added dropwise under stirring to form a homogeneous gel with a molar composition of 1 SiO_2: 0.3 ADA: 0.2 NaOH: 100 H_2O. Pre-synthesized DDR zeolite crystals (1 wt% relative to SiO_2 content), prepared according to a reported procedure [38], were then added in the gel as seeds and the mixture was stirred for 1 h. The seeded gel was transferred into a Teflon-lined autoclave and subjected to hydrothermal treatment at 160 °C for 48 h. After crystallization, the product was washed with deionized water until neutral pH was achieved, followed by overnight drying to obtain DDR zeolite crystals. Finally, the DDR crystals were ball-milled at 500 rpm for 24 h using a planetary ball mill (Miqi YXQM-1L). The milled product was subsequently dispersed in deionized water and subjected to sedimentation overnight to remove larger and un-milled particles. Submicron DDR zeolite seeds in the supernatant were then collected by centrifugation and drying for membrane seeding.

CHA zeolite seeds were prepared through an interzeolite conversion process using USY zeolite as the starting material. In a typical synthesis, USY zeolite (Si/Al = 40) and water was dispersed in the TMAdaOH solution under stirring at room temperature to obtain a homogeneous gel with a molar composition of 1 SiO_2: 0.0125 Al_2O_3: 0.142 TMAdaOH: 5 H_2O. The resulting gel was transferred to a Teflon-lined stainless steel autoclave and subjected to hydrothermal crystallization at 175 °C for 16 days. After crystallization, the solid product was collected by centrifugation, washed with deionized water, and dried overnight to obtain the CHA zeolite seeds.

2.3. Synthesis of DDR zeolite membranes

DDR zeolite membranes were synthesized on porous α-Al_2O_3 supports using a secondary growth approach. The supports were first seeded via vacuum filtration with 1 mL of a 2 $mg{\cdot}mL^{-1}$ seed solution of either DDR or CHA, followed by calcination in air at 550 °C for 6 h. For membrane growth, the seeded supports were vertically placed in a 50 mL Teflon-lined autoclave containing a synthesis gel with a molar composition of 1 SiO_2: *x* ADA: 0.5 EDA: 40 H_2O (*x* = 0.03 or 0.05). Hydrothermal crystallization was conducted at 140 °C for 44–96 h in a preheated oven. The resulting membranes were rinsed with deionized water, dried at 115 °C overnight, and finally calcined at 550 °C for 6 h to remove the template, with a heating and cooling rate of 1 $°C{\cdot}min^{-1}$, to obtain the final DDR zeolite membranes.

2.4. Pervaporation dehydration testing

Fig. 1 shows a schematic diagram of the experimental setup used for the pervaporation dehydration tests. The prepared DDR zeolite membranes were mounted into a custom-built membrane module using O-rings to ensure a gas-tight sealing. For testing, the feed side of the system was maintained at atmospheric pressure and was fed with an aqueous LiBr solution (20–60 wt%). The permeate side was connected to a liquid nitrogen cold trap, which was kept under vacuum (<10 Pa) by a vacuum pump to condense and thereby collect the permeate stream. The LiBr concentration in the permeate was quantified by conductivity measurements using a calibrated meter. Membrane performance was evaluated based on the water permeation flux (*J*) and the salt rejection (*R*), which were calculated using the following equations:

$$J = \frac{m}{A{\cdot}t} \tag{1}$$

$$R = \frac{C_f - C_p}{C_f} \times 100\% \tag{2}$$

where *m* represents the mass of the permeated water, *A* is the membrane area, *t* is the test time, and C_f and C_p are the LiBr concentrations in the

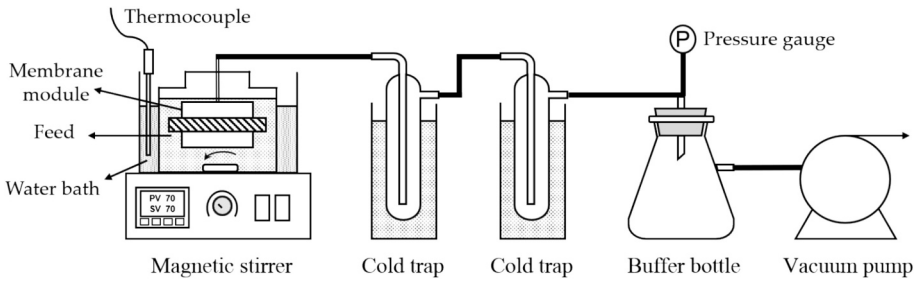

Fig. 1. Schematic diagram of the experimental setup used for the pervaporation dehydration tests.

feed and permeate streams, respectively.

2.5. Characterization

Scanning electron microscope (SEM) images and energy-dispersive X-ray spectroscopy (EDX) mapping were performed on a COXEM EM-30PLUS electron microscope. X-ray diffraction (XRD) patterns were obtained using a Bruker D8 ADVANCE X-ray diffractometer.

3. Results and discussion

3.1. Fabrication of zeolite seeds and seeded supports

Fig. 2 presents the morphological and crystallographic characteristics of the synthesized zeolite seeds. The as-prepared seeds (Fig. 2a) exhibited uniform particle morphology with an average particle size of approximately 1 μm. Their corresponding XRD pattern (Fig. 2b) confirmed a pure DDR-type phase without detectable impurities. Mechanical ball milling effectively reduced the particle size to 200–800 nm (inset, Fig. 2a). Subsequent size fractionation via gravitational settling yielded a uniform seed layer with a thickness of 1–2 μm onto the α-Al_2O_3 support (Fig. 3a, b).

In parallel, the prepared CHA zeolite seeds consisted of monodisperse submicron particles with a diameter of approximately 150 nm (Fig. 2c) and exhibited phase-pure CHA crystallinity, as confirmed by the absence of any USY zeolite diffraction peaks in the XRD pattern (Fig. 2d). The resulting CHA seed layer was of comparable quality and thickness to the DDR seed layer (Fig. 3c, d). Both layers were highly uniform, making them well-suited for the subsequent secondary growth of DDR zeolite membranes in comparative studies.

3.2. Heteroepitaxial growth of DDR zeolite membranes

To suppress impurity zeolite phase formation in DDR zeolite membranes, methyltropinium iodide (MTI) has been proposed as an alternative template to ADA [39]. Although MTI enables the preparation of high-quality, pure-phase DDR membranes via secondary growth, its limited commercial availability hinders large-scale application. In parallel, the choice of zeolite seeds has been shown to substantially influence the growth of DDR membranes. Zheng et al. [40] reported that ball-milled aluminum-containing DDR zeolite (Sigma-1) seeds promoted the rapid synthesis of phase-pure DDR zeolite, whereas non-milled Sigma-1 seeds and conventional all-silica DDR (DD3R) zeolite seeds led to slower crystallization kinetics and higher impurity content. Given the difficulty in directly preparing nano-sized DDR seeds, Jeong et al. [35] successfully employed SSZ-13 (CHA-type) zeolite seeds for the heteroepitaxial growth of DDR membranes using MTI as the template, capitalizing on the structural compatibility between the CHA and DDR frameworks.

It should be noted that DDR zeolite seeds may contain trace SGT impurities due to the strong co-crystallization tendency of the two

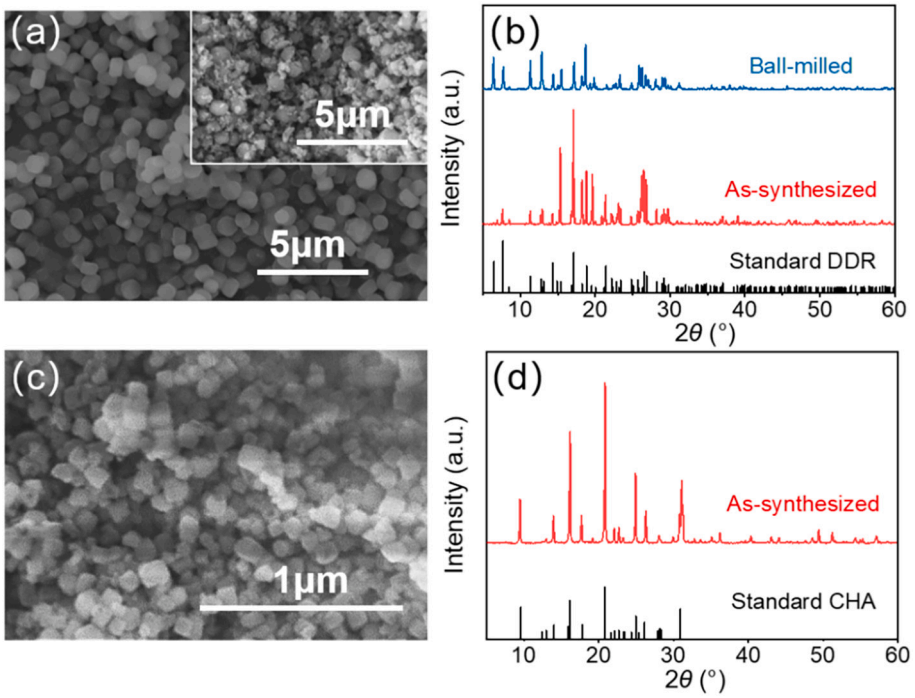

Fig. 2. SEM images and XRD patterns of (a, b) DDR zeolite and (c, d) CHA zeolite. The inset in Fig. 2a is the SEM image of DDR zeolite after ball-milling.

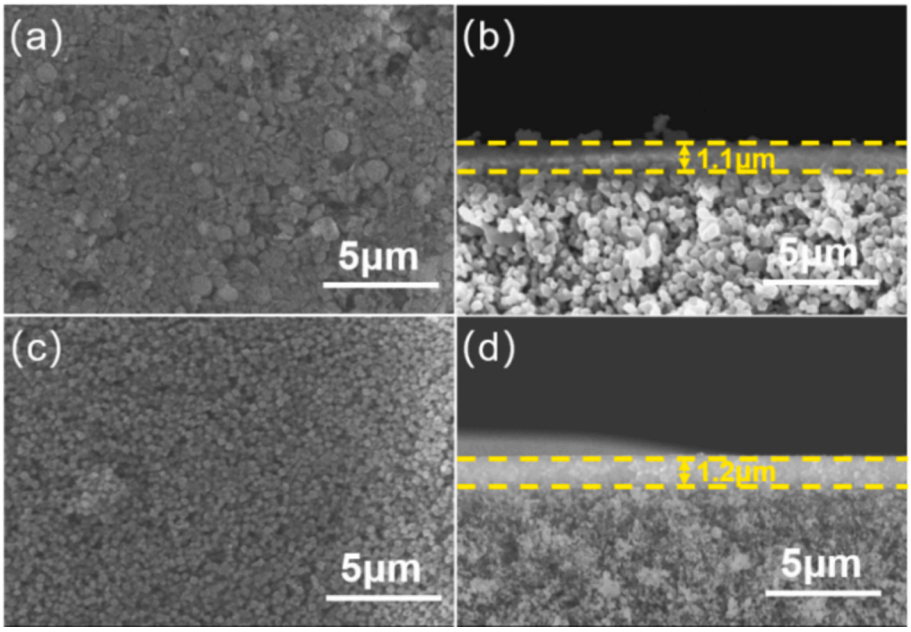

Fig. 3. Top-view and cross-sectional SEM images of α-Al_2O_3 supports seeded with (a, b) DDR and (c, d) CHA zeolite seeds.

phases under ADA templating. Given this potential impurity issue and the structural compatibility between CHA and DDR zeolites, we reasoned that employing CHA seeds, which are entirely free of the SGT phase, could suppress SGT zeolite formation during the secondary growth of DDR zeolite membranes, even in an ADA-based system. Therefore, we extended the heteroepitaxial growth strategy to fabricate phase-pure DDR membranes using commercially available ADA as the template. Fig. 4 shows SEM images of DDR zeolite membranes prepared using DDR and CHA seed layers. In addition to the relatively small DDR zeolite crystals, the membrane grown on DDR seeds exhibited some large grains (~10 μm in diameter) (Fig. 4a), which were identified as SGT-type zeolite by XRD (Fig. 5a). Significant gel infiltration into the support was also observed (Fig. 4b), resulting in an effective zeolite layer thickness of merely 2.5 μm. In contrast, membranes prepared with CHA seeds displayed improved surface coverage, consisting of uniform rhombus-shaped DDR crystals with no detectable SGT grains (Fig. 4c). XRD confirmed the high phase purity, showing exclusively DDR-type diffraction peaks with negligible contributions from CHA or SGT phases (Fig. 5b). Cross-sectional imaging indicated that gel penetration remained considerable during heteroepitaxial growth, yielding a similarly thin zeolite layer (Fig. 4d). These results demonstrate that the heteroepitaxial approach using CHA seeds provides an effective pathway to fabricate high-quality DDR zeolite membranes with the industrially viable ADA template. This improvement can be likely attributed to the complete absence of SGT impurities in the CHA seeds and the structural compatibility between the CHA and DDR frameworks, which collectively favor the heteroepitaxial growth of phase-pure DDR structure.

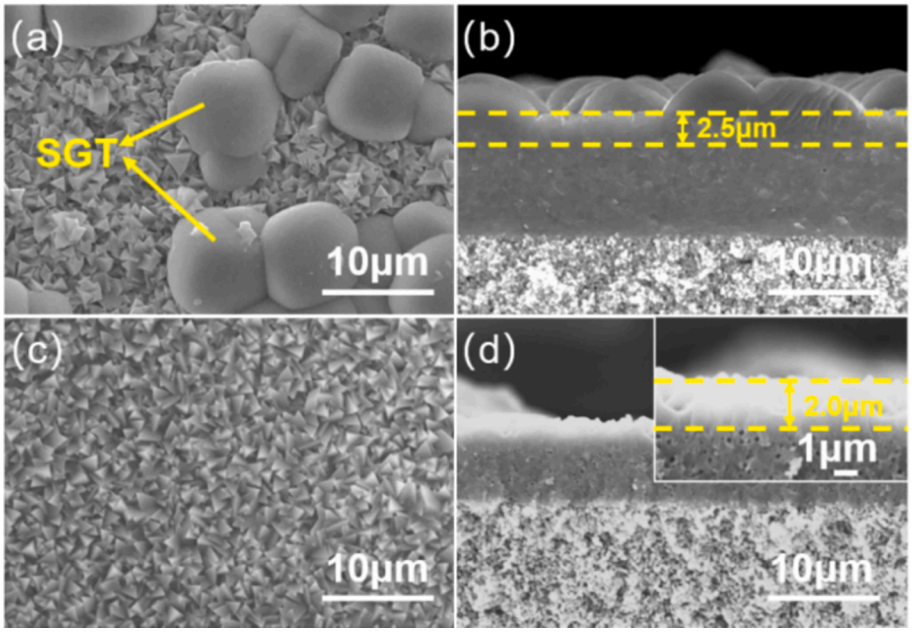

Fig. 4. Top-view and cross-sectional SEM images of DDR zeolite membranes prepared using (a, b) DDR and (c, d) CHA zeolites as seeds with an ADA/SiO_2 molar ratio of 0.03 in the gel at 140 °C for 44 h.

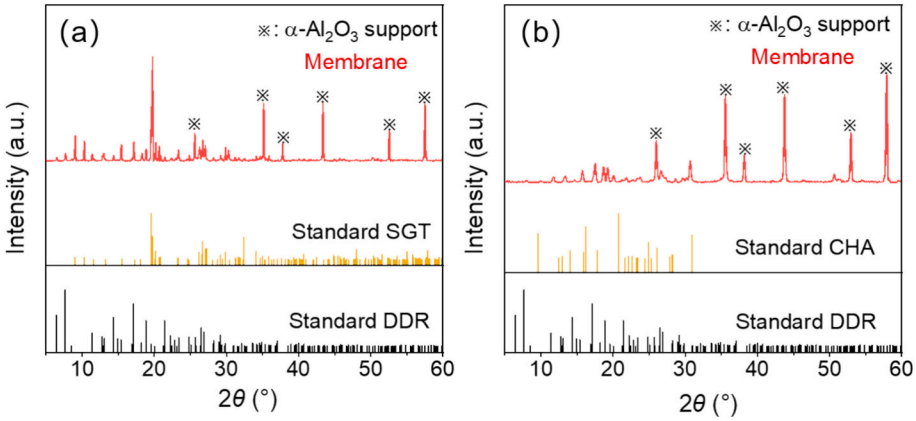

Fig. 5. XRD patterns of DDR zeolite membranes prepared using (a) DDR and (b) CHA zeolites as seeds with an ADA/SiO_2 molar ratio of 0.03 in the gel at 140 °C for 44 h.

To further promote the intergrowth of DDR zeolite crystals within the membrane, the crystallization time was extended from 44 to 96 h to investigate its effect on membrane quality. Prior to membrane activation, He permeance measurements (Table 1) yielded values ranging from 2.1×10^{-10} to 7.0×10^{-8} mol·m^{-2}·s^{-1}·Pa^{-1}, indicating the presence of grain boundary defects with varying severity in membranes. The detectable He permeance suggests that complete elimination of grain boundary defects remains challenging, likely due to incomplete intergrowth of DDR crystals (Fig. 6a–c). Cross-sectional SEM analysis (Fig. 6d–f) revealed substantial penetration of the precursor gel into the porous support layer. The resulting DDR zeolite top layers remained relatively thin (1–2 μm) regardless of synthesis time. Importantly, no impurity phases were detected under any of the synthesis conditions, demonstrating the exceptional phase purity achieved by the CHA-seeded heteroepitaxial growth method. This represents a significant advantage over conventional DDR-seeded approaches, which are prone to the formation of DOH-type zeolite impurities under prolonged synthesis durations [36].

In another attempt to enhance membrane quality, the ADA/SiO_2 ratio in the synthesis gel was increased from 0.03 to 0.05. As illustrated in Fig. 7, this adjustment led to substantial improvements in membrane morphology and integrity. The resulting DDR zeolite crystals showed excellent intergrowth, forming a continuous layer with a thickness of 4.3 μm, which is much thicker than membranes synthesized at the lower ADA/SiO_2 ratio of 0.03 (1–2 μm). The increased membrane thickness is likely attributable to accelerated crystal growth kinetics under higher template concentrations. The cross-sectional EDX mapping revealed a notably low Al content within the zeolite layer, thus confirming that Al leaching from the α-Al_2O_3 support was insignificant. XRD analysis further confirmed the phase purity, showing a well-defined DDR structure without detectable SGT impurities. The exceptional phase purity of the DDR zeolite membrane highlights the distinctive benefits of the heteroepitaxial growth strategy. Additionally, permeation tests demonstrated that the membrane was complete He-impermeable before activation, suggesting negligible grain boundary defects. These high-quality membranes were subsequently employed for pervaporation dehydration studies of LiBr solutions, as described in the following section.

Table 1
He permeances of as-prepared DDR zeolite membranes without activation.

Crystallization time (h)	44	60	72	96
He permeance (10^{-8} mol·m^{-2}·s^{-1}·Pa^{-1})	0.3	7.0	0.077	0.021

3.3. Pervaporation dehydration of LiBr solutions using DDR zeolite membranes

Fig. 8 illustrates the temperature-dependent pervaporation performance of a DDR zeolite membrane for dehydrating LiBr solutions. The water flux exhibited a strong positive correlation with temperature across all LiBr concentrations tested (20–60 wt%). This trend, as commonly observed in pervaporation dehydration regardless of membrane materials [22–26], is primarily attributed to the increased water vapor pressure gradient across the membrane at higher temperatures, which serves as the fundamental driving force for permeation. Notably, the extent of flux enhancement with temperature became less pronounced at higher LiBr concentrations. For the 20 wt% LiBr solution, water flux increased markedly from 0.37 kg·m^{-2}·h^{-1} at 20 °C to 1.56 kg·m^{-2}·h^{-1} at 80 °C, representing a 321% increase. In comparison, the 60 wt% solution exhibited only a 100% rise (from 0.16 to 0.32 kg·m^{-2}·h^{-1}) over the same temperature range. This concentration-dependent behavior can be mainly explained by the considerably reduced water activity in highly concentrated LiBr solutions. Importantly, the membranes maintained excellent LiBr rejection (>99%) throughout all experimental conditions, demonstrating high-quality of the synthesized DDR zeolite membrane.

The temperature dependence of water permeation flux follows Arrhenius-type behavior, as expressed by Eq. (3):

$$J = J_0 \, exp\left(-\frac{\Delta E_a}{RT}\right) \tag{3}$$

where J represents the water flux, J_0 is the pre-exponential factor, E_a is the activation energy for water permeation, R is the universal gas constant, T is the absolute temperature. Accordingly, the activation energy E_a for water transport through the DDR zeolite membrane can be determined from the slope of the linear fit to an Arrhenius plot of ln$J$ versus $1/T$.

Fig. 9 shows Arrhenius plots of water permeation flux through the DDR zeolite membrane. The calculated activation energies for water permeation exhibited a pronounced dependence on LiBr concentration, as summarized in Table 2. Notably, the activation energy decreased substantially from 20.64 kJ·mol^{-1} for 20 wt% LiBr solutions to 9.69 kJ·mol^{-1} for 60 wt% LiBr solutions, suggesting the LiBr concentration significantly affected water transport through the membrane.

The transport of water through microporous membranes during pervaporation is commonly described by an adsorption–diffusion mechanism, represented by the following equation [41]:

$$J = S_0 \, exp\left(\frac{\Delta H_s}{RT}\right) D_0 \, exp\left(-\frac{E_D}{RT}\right) \frac{\Delta P}{L} \tag{4}$$

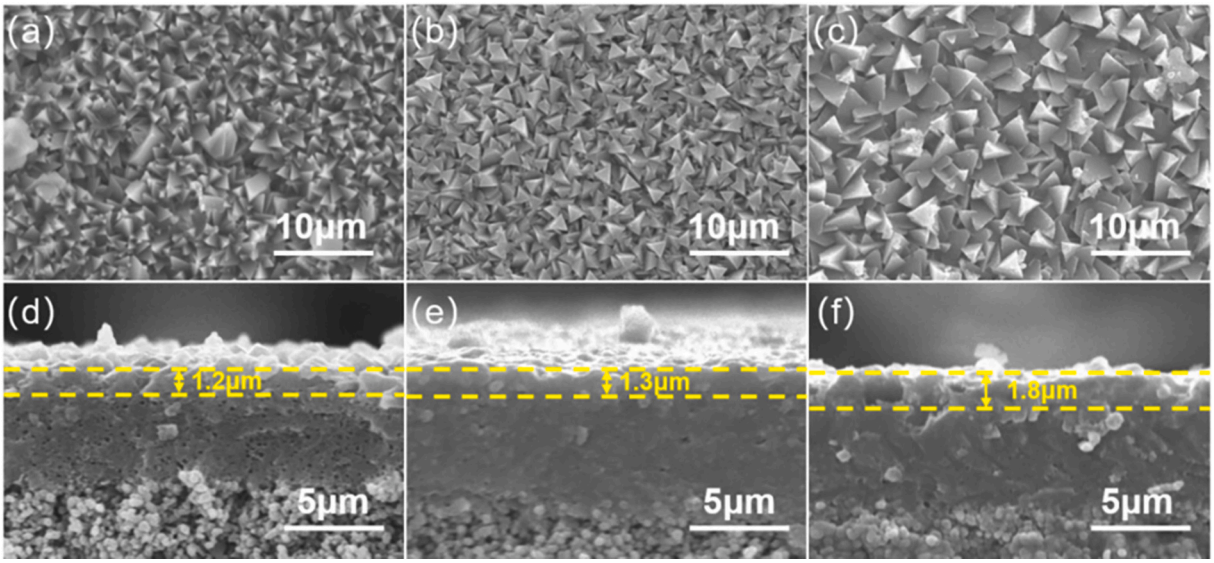

Fig. 6. Top-view and cross-sectional SEM images of DDR zeolite membranes prepared using CHA zeolite as seeds with an ADA/SiO_2 molar ratio of 0.03 in the gel at 140 °C for (a, d) 60, (b, e)72 and (c, f) 96 h.

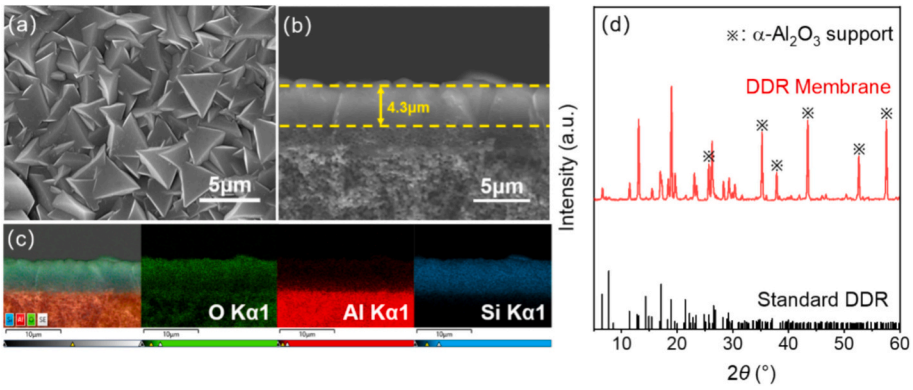

Fig. 7. Characterization of a DDR zeolite membrane prepared using CHA zeolite seeds from a gel with an ADA/SiO_2 molar ratio of 0.05 at 140 °C for 96 h: (a) top-view and (b) cross-sectional SEM images, (c) cross-sectional EDX mapping, and (d) XRD pattern.

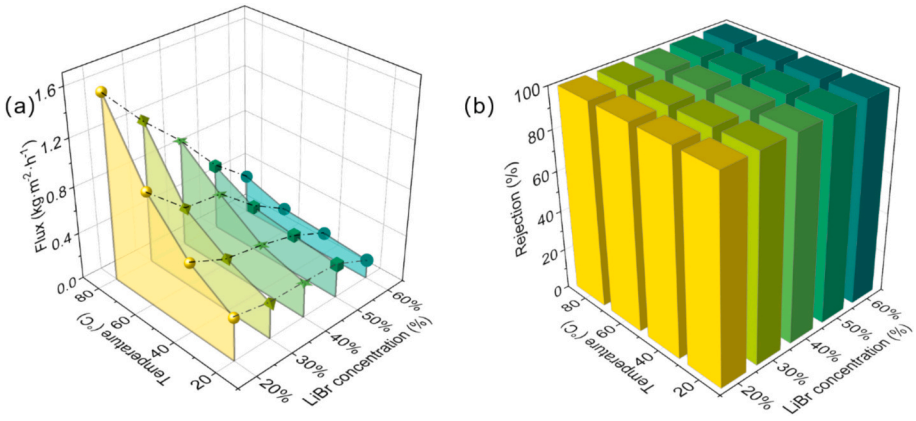

Fig. 8. (a) Flux and (b) rejection of a DDR zeolite membrane for pervaporation dehydration of LiBr solutions with different concentrations and temperatures.

where J represents the water permeation flux, S_0 and D_0 are pre-exponential factors, ΔH_s is the heat of adsorption, E_D is the activation energy for diffusion, L is the effective membrane thickness, R is the universal gas constant, T is the testing temperature, ΔP is the water vapor partial pressure between the feed and permeate sides. Since the water vapor partial pressure on the permeate side was negligible, ΔP can be expressed as Eq. (5) based on the Clausius-Clapeyron equation, as follows:

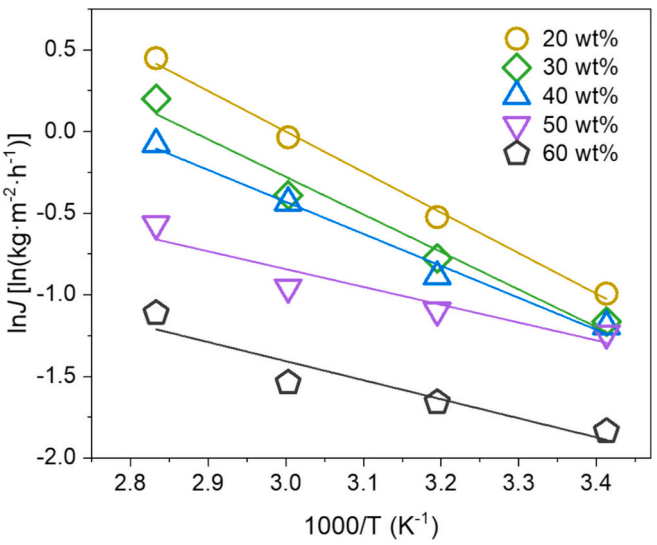

Fig. 9. Arrhenius plots of water permeation flux through the DDR zeolite membrane during pervaporation dehydration of LiBr solutions at varying concentrations.

Table 2
Activation energies for water permeation through the DDR zeolite membrane in LiBr solutions at varying concentrations.

LiBr concentration (wt%)	20	30	40	50	60
E_a (kJ·mol^{-1})	20.64	19.12	16.30	9.06	9.69

$$\Delta P = P_f = k_0\, exp\left(-\frac{\Delta H^{vap}}{RT}\right) \tag{5}$$

where P_f is the water vapor pressure on the feed side, k_0 is the pre-exponential factor, ΔH^{vap} is the enthalpy of vaporization. The integration of Eqs. (4) and (5) yields the water permeation flux expression given in Eq. (6).

$$J = \frac{k_0 S_0 D_0}{L}\, exp\left(-\frac{E_D - \Delta H_s + \Delta H^{vap}}{RT}\right) \tag{6}$$

By combination of Eqs. (3) and (6), the activation energy (ΔE_a) for water permeation can be expressed as follows:

$$\Delta E_a = E_D - \Delta H_s + \Delta H^{vap} \tag{7}$$

The observed decrease in the activation energy (ΔE_a) for water permeation with increasing LiBr concentration primarily arises from the combined influence of the strongly concentration-dependent thermodynamic properties of LiBr solutions and the adsorption behaviors of the membrane. Specifically, higher LiBr concentrations strengthen the ion-water interactions, thereby raising the enthalpy of vaporization (ΔH^{vap}) of water. In contrast, E_D is expected to remain largely constant because the membrane pore size is fixed. Therefore, as quantitatively described by Eq. (7), the net decrease in ΔE_a must be attributed to changes in the adsorption term, ΔH_s. This is because the extremely low water activity in concentrated LiBr solutions significantly reduces the adsorption coverage on the zeolite, which in turn causes ΔH_s to increase as the coverage decreases [42]. Consequently, the ΔH_s term in Eq. (7) increases rapidly at high salt concentrations, which dominantly drives down the overall ΔE_a. Although this framework accounts for the lowered energy barrier for membrane permeation, it also highlights a fundamental challenge in dehydrating concentrated LiBr solutions, that is, the same strong ion–water interactions that largely reduce ΔE_a also increase the energy required for extracting water from the bulk solution. This trade-off directly results in markedly reduced water fluxes at higher LiBr concentrations (e.g., 0.16 to 0.32 kg·m^{-2}·h^{-1} for 60 wt% LiBr versus 0.37 to 1.5 kg·m^{-2}·h^{-1} for 20 wt% LiBr across 20–80 °C). In summary, the coupling between solution thermodynamics and membrane adsorption behavior strongly dictates the overall permeation performance in hypersaline LiBr systems.

Fig. 10 shows the operational stability of the DDR zeolite membrane during pervaporation dehydration of a 60 wt% LiBr solution at 80 °C. Throughout the entire 48-h testing period, the membrane maintained a consistent water flux of approximately 0.33 kg·m^{-2}·h^{-1} while achieving salt rejection exceeding 99.9 %, demonstrating exceptional stability in handling highly concentrated LiBr solutions. These results indicate that DDR zeolite membranes offer a promising alternative for the development of novel membrane-based desorbers in LiBr–H_2O absorption chillers, potentially enabling more compact and efficient system designs.

4. Conclusions

High-quality DDR zeolite membranes were successfully fabricated through heteroepitaxial growth using CHA zeolite seeds for LiBr solution dehydration via pervaporation. Our findings reveal that the zeolite seed type plays a critical role in DDR membrane secondary growth, where employing CHA seeds instead of conventional DDR seeds effectively suppressed the competitive SGT phase formation, ultimately yielding high-quality DDR membranes. The fabricated DDR zeolite membrane demonstrated water fluxes ranging from 0.16 to 1.56 kg·m^{-2}·h^{-1} during pervaporation dehydration of 20–60 wt% LiBr solutions across a temperature range of 20–80 °C. Remarkably, LiBr rejection consistently exceeded 99.9 % regardless of operating temperature and solution concentration. Notably, the activation energy for water permeation decreased with increasing LiBr concentration, attributed to the combined effect of the thermodynamic properties of LiBr solutions and the adsorption properties of the membrane. The membranes exhibited exceptional operational stability, maintaining consistent performance during 48 h of tests under conditions of 80 °C and 60 wt% LiBr concentration. These results highlight the significant potential of DDR zeolite membranes for application in LiBr-H_2O absorption chiller systems, particularly for handling hypersaline LiBr streams.

CRediT authorship contribution statement

Zilin Pan: Writing – original draft, Investigation, Formal analysis, Data curation. **Feng Ye:** Writing – original draft, Investigation. **Shuanshi Fan:** Writing – review & editing. **Yanhong Wang:** Writing – review & editing. **Xuemei Lang:** Writing – review & editing. **Lisha Lu:** Investigation, Formal analysis, Data curation. **Gang Li:** Writing – review

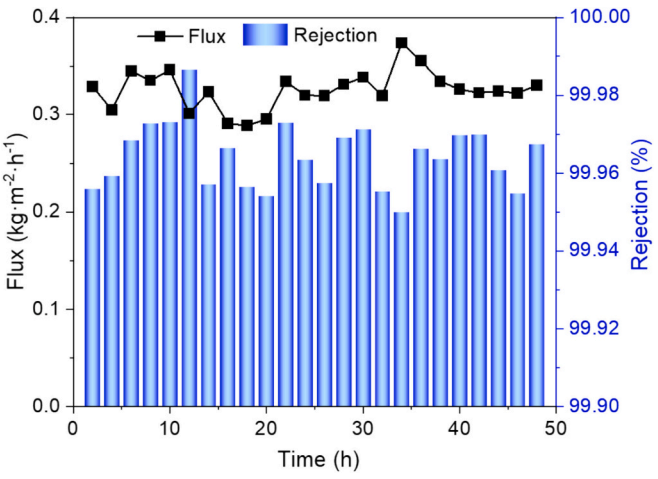

Fig. 10. Time course of pervaporation dehydration of a 60 wt% LiBr solution at 80 °C using the DDR zeolite membrane.

& editing, Conceptualization.

Declaration of competing interest

The authors declare that they have no known competing financial interests or personal relationships that could have appeared to influence the work reported in this paper.

Acknowledgements

We acknowledge the financial support from the Fundamental Research Funds for the Central Universities (grant Nos. 2024ZYGXZR100 and 2025ZYGXZR098) and the Guangdong Basic and Applied Basic Research Foundation (grant No. 2022A151501206).

Data availability

Data will be made available on request.

References

[1] Z. Li, J. Liu, Appropriate heat load ratio of generator for different types of air cooled lithium bromide-water double effect absorption chiller, Energy Convers. Manage. 99 (2015) 264–273, https://doi.org/10.1016/j.enconman.2015.04.055.
[2] S. Du, Z. Xu, R. Wang, C. Yang, Development of direct seawater-cooled LiBr–H_2O absorption chiller and its application in industrial waste heat utilization, Energy 294 (2024) 130816, https://doi.org/10.1016/j.energy.2024.130816.
[3] R. Palacios-Bereche, R. Gonzales, S.A. Nebra, Exergy calculation of lithium bromide-water solution and its application in the exergetic evaluation of absorption refrigeration systems LiBr-H_2O, Int. J. Energy Res. 36 (2012) 166–181, https://doi.org/10.1002/er.1790.
[4] M. Lickley, S. Solomon, S. Fletcher, G.J.M. Velders, J. Daniel, M. Rigby, S. A. Montzka, L.J.M. Kuijpers, K. Stone, Quantifying contributions of chlorofluorocarbon banks to emissions and impacts on the ozone layer and climate, Nat. Commun. 11 (2020) 1380, https://doi.org/10.1038/s41467-020-15162-7.
[5] D.K. Papanastasiou, A. Beltrone, P. Marshall, J.B. Burkholder, Global warming potential estimates for the C1-C3 hydrochlorofluorocarbons (HCFCs) included in the Kigali Amendment to the Montreal Protocol, Atmos. Chem. Phys. 18 (2018) 6317–6330, https://doi.org/10.5194/acp-18-6317-2018.
[6] M.K. Vollmer, J. Mühle, S. Henne, D. Young, M. Rigby, B. Mitrevski, S. Park, C. R. Lunder, T.S. Rhee, C.M. Harth, M. Hill, R.L. Langenfelds, M. Guillevic, P. M. Schlauri, O. Hermansen, J. Arduini, R.H.J. Wang, P.K. Salameh, M. Maione, P. B. Krummel, S. Reimann, S. O'Doherty, P.G. Simmonds, P.J. Fraser, R.G. Prinn, R. F. Weiss, L. Paul Steele, Unexpected nascent atmospheric emissions of three ozone-depleting hydrochlorofluorocarbons, Proc. Natl. Acad. Sci. 118 (2021) 2010914118, https://doi.org/10.1073/pans.2010914118.
[7] R. Zhai, X. Li, Y. Zhuang, B. Ye, X. Liu, Q. Li, L. Tang, K. Wang, Study on the flame retarding mechanism of HFC-134a on hydrocarbon refrigerants, Int. J. Refrig. 174 (2025) 1–13, https://doi.org/10.1016/j.ijrefrig.2025.02.018.
[8] W.T. Tsai, An overview of environmental hazards and exposure risk of hydrofluorocarbons (HFCs), Chemosphere 61 (2005) 1539–1547, https://doi.org/10.1016/j.chemosphere.2005.03.084.
[9] X. Wang, H.T. Chua, Absorption cooling: a review of lithium bromide-water chiller technologies, Recent Pat. Mech. Eng. 2 (2010) 193–213, https://doi.org/10.2174/1874477X10902030193.
[10] F. Ziegler, State of the art in sorption heat pumping and cooling technologies, Int. J. Refrig. 25 (2002) 450–459, https://doi.org/10.1016/S0140-7007(01)00036-6.
[11] A.H.H. Ali, Design of a compact absorber with a hydrophobic membrane contactor at the liquid-vapor interface for lithium bromide-water absorption chillers, Appl. Energy 87 (2010) 1112–1121, https://doi.org/10.1016/j.apenergy.2009.05.018.
[12] S.Y. Lee, S.K. Lee, J.T. Chung, Y.T. Kang, Numerical evaluation of a compact generator design for steam driven H_2O/LiBr absorption chiller application, Energy 152 (2018) 512–520, https://doi.org/10.1016/j.energy.2018.03.161.
[13] T. Hu, X. Xie, Y. Jiang, Design and experimental study of a plate-type falling-film generator for a LiBr/H_2O absorption heat pump, Int. J. Refrig. 74 (2017) 302–310, https://doi.org/10.1016/j.ijrefrig.2016.09.024.
[14] Z. Sui, W. Wu, A comprehensive review of membrane-based absorbers/desorbers towards compact and efficient absorption refrigeration systems, Renew. Energy 201 (2022) 563–593, https://doi.org/10.1016/j.renene.2022.10.115.
[15] C. Zhai, W. Wu, A. Coronas, Membrane-based absorption cooling and heating: development and perspectives, Renew. Energy 177 (2021) 663–688, https://doi.org/10.1016/j.renene.2021.05.156.
[16] J. Ibarra-Bahena, S. Raman, Y.R. Galindo-Luna, A. Rodríguez-Martínez, W. Rivera, Role of membrane technology in absorption heat pumps: a comprehensive review, Membranes 10 (2020) 1–28, https://doi.org/10.3390/membranes10090216.
[17] S.J. Hong, E. Hihara, C. Dang, Novel absorption refrigeration system with a hollow fiber membrane-based generator, Int. J. Refrig. 67 (2016) 418–432, https://doi.org/10.1016/j.ijrefrig.2016.04.012.
[18] M. Venegas, N. García-Hernando, M. de Vega, A parametric analysis on the effect of design and operating variables in a membrane-based desorber, Int. J. Refrig. 99 (2019) 47–58, https://doi.org/10.1016/j.ijrefrig.2018.11.043.
[19] Z. Wang, Z. Gu, S. Feng, Y. Li, Application of vacuum membrane distillation to lithium bromide absorption refrigeration system, Int. J. Refrig. 32 (2009) 1587–1596, https://doi.org/10.1016/j.ijrefrig.2009.07.002.
[20] J. Ibarra-Bahena, W. Rivera, S.D. Nanco-Mejía, R.J. Romero, E. Venegas-Reyes, U. Dehesa-Carrasco, Experimental performance of a membrane desorber operating under simulated warm weather condensation temperatures, Membranes 11 (2021) 474, https://doi.org/10.3390/membranes11070474.
[21] C. Algieri, E. Drioli, Zeolite membranes: synthesis and applications, Sep. Purif. Technol. 278 (2021) 119295, https://doi.org/10.1016/j.seppur.2021.119295.
[22] L. Wang, J. Yang, J. Wang, Microwave synthesis of NaA zeolite membranes on coarse macroporous α-Al_2O_3 tubes for desalination, Microporous Mesoporous Mater. 306 (2020) 110360, https://doi.org/10.1016/j.micromeso.2020.110360.
[23] C.H. Cho, K.Y. Oh, S.K. Kim, J.G. Yeo, P. Sharma, Pervaporative seawater desalination using NaA zeolite membrane: mechanisms of high water flux and high salt rejection, J. Membr. Sci. 371 (2011) 226–238, https://doi.org/10.1016/j.memsci.2011.01.049.
[24] M. Drobek, C. Yacou, J. Motuzas, A. Julbe, L. Ding, J.C. Diniz da Costa, Long term pervaporation desalination of tubular MFI zeolite membranes, J. Membr. Sci. 415–416 (2012) 816–823, https://doi.org/10.1016/j.memsci.2012.05.074.
[25] C. Zhou, J. Zhou, A. Huang, Seeding-free synthesis of zeolite FAU membrane for seawater desalination by pervaporation, Microporous Mesoporous Mater. 234 (2016) 377–383, https://doi.org/10.1016/j.micromeso.2016.07.050.
[26] H. Zhang, L. Gan, N. Liu, X. Huang, N. Hu, X. Chen, Ionothermal synthesis of CHA-type zeolite membrane for desalination, J. Chin. Ceram. Soc. 50 (2022) 1375–1384, https://doi.org/10.14062/J.ISSN.0454-5648.20210599.
[27] L. Yu, N. Al-Jariry, T. Serikbayeva, J. Hedlund, Ultra-thin zeolite CHA and FAU membranes for desalination by pervaporation, Sep. Purif. Technol. 294 (2022) 121177, https://doi.org/10.1016/j.seppur.2022.121177.
[28] F. Asdrubali, S. Grignaffini, Experimental evaluation of the performances of a H_2O-LiBr absorption refrigerator under different service conditions, Int. J. Refrig. 28 (2005) 489–497, https://doi.org/10.1016/j.ijrefrig.2004.11.006.
[29] J. Kuhn, J. Gascon, J. Gross, F. Kapteijn, Detemplation of DDR type zeolites by ozonication, Microporous Mesoporous Mater. 120 (2009) 12–18, https://doi.org/10.1016/j.micromeso.2008.09.018.
[30] J. Zhang, J. Liang, H. Peng, Y. Mi, P. Luo, H. Xu, M. He, P. Wu, Cost-effective fast-synthesis of chabazite zeolites for the reduction of NO_x, Appl. Catal. B 292 (2021) 120163, https://doi.org/10.1016/j.apcatb.2021.120163.
[31] Y. Zhou, P. Du, Z. Song, X. Zhang, Y. Liu, Y. Zhang, X. Gu, Synthesis of thin DD3R zeolite membranes on hollow fibers using gradient-centrifuged seeds for CO_2/CH_4 separation, J. Membr. Sci. Lett. 3 (2023) 100038, https://doi.org/10.1016/j.memlet.2023.100038.
[32] E. Hayakawa, S. Himeno, Synthesis of a DDR-type zeolite membrane by using dilute solutions of various alkali metal salts, Sep. Purif. Technol. 218 (2019) 89–96, https://doi.org/10.1016/j.seppur.2019.02.015.
[33] P.N.X. Vo, P.D. Phan, P.T. Ngo, N. Le-Phuc, T.V. Tran, T.N. Luong, A. Wotzka, D. Seeburg, S. Wohlrab, Memory effect in DDR zeolite powder and membrane synthesis, Microporous Mesoporous Mater. 279 (2019) 142–152, https://doi.org/10.1016/j.micromeso.2018.12.031.
[34] X. Han, W. Xu, F. Meng, Z. Liu, C. Liao, Recent advances in zeolite membranes for gas separation and pervaporation in petrochemicals, J. Mater. Chem. A 13 (2025) 10358–10387, https://doi.org/10.1039/D4TA08746A.
[35] Y. Jeong, S. Hong, E. Jang, E. Kim, H. Baik, N. Choi, A.C.K. Yip, J. Choi, An hetero-epitaxially grown zeolite membrane, Angew. Chem. Int. Ed. 58 (2019) 18654–18662, https://doi.org/10.1002/ANIE.201911164.
[36] M. Wang, L. Bai, M. Li, L. Gao, M. Wang, P. Rao, Y. Zhang, Ultrafast synthesis of thin all-silica DDR zeolite membranes by microwave heating, J. Membr. Sci. 572 (2019) 567–579, https://doi.org/10.1016/j.memsci.2018.11.049.
[37] X. Wang, Y. Zhang, X. Wang, E. Andres-Garcia, P. Du, L. Giordano, L. Wang, Z. Hong, X. Gu, S. Murad, F. Kapteijn, Xenon recovery by DD3R zeolite membranes: application in anaesthetics, Angew. Chem. Int. Ed. 58 (2019) 15518–15525, https://doi.org/10.1002/anie.201909544.
[38] N. Xu, D. Meng, X. Tang, X. Kong, L. Kong, Y. Zhang, H. Qiu, M. Wang, Y. Zhang, Fast synthesis of thin all-silica DDR zeolite membranes with inorganic base as mineralizing agent for CO_2-CH_4 separation, Sep. Purif. Technol. 253 (2020) 117505, https://doi.org/10.1016/j.seppur.2020.117505.
[39] E. Hayakawa, S. Himeno, Synthesis of all-silica ZSM-58 zeolite membranes for separation of CO_2/CH_4 and CO_2/N_2 gas mixtures, Microporous Mesoporous Mater. 291 (2020) 109695, https://doi.org/10.1016/j.micromeso.2019.109695.
[40] F. Zheng, W. Jing, X. Gu, N. Xu, J. Dong, Rapid synthesis of pure DD3R zeolite using ball-milled Sigma-1 seeds under static conditions, J. Mater. Sci. 48 (2013) 6286–6292, https://doi.org/10.1007/S10853-013-7428-0.
[41] B. Bettens, S. Dekeyzer, B. Van Der Bruggen, J. Degrève, C. Vandecasteele, Transport of pure components in pervaporation through a microporous silica membrane, J. Phys. Chem. B 109 (2005) 52165222, https://doi.org/10.1021/jp044515E.
[42] V. Bolis, C. Busco, P. Ugliengo, Thermodynamic study of water adsorption in high-silica zeolites, J. Phys. Chem. B 110 (2006) 14849–14859, https://doi.org/10.1021/jp061078q.